PSFC/RR-09-12

Magnetics R&D – Task D&T-01

MIT Cooperative Agreement
Final Report For FY2009

September 18, 2009

J.V. Minervini, M. Takayasu, J.H. Schultz, J. Feng, L. Chiesa,

TABLE OF CONTENTS

Magnetics R&D – Task D&T-01

MIT Cooperative Agreement
Final Report For FY2009

Principal Investigator:	Co-Principal Investigator:
Joseph V. Minervini MIT Plasma Science and Fusion Center NW22-129 Cambridge, MA 02139 Tel: (617) 253-5503 Fax: (617) 253-0807 minervini@psfc.mit.edu	Makoto Takayasu MIT Plasma Science and Fusion Center NW22-109 Cambridge, MA 02139 Tel: (617) 253-8358 Fax: (617) 253-0807 takayasu@psfc.mit.edu

1 PROJECT SUMMARY

The Fusion Technology and Engineering Division (FTED) of the MIT Plasma Science and Fusion Center (PSFC) completes the second year of a five year cooperative agreement at the end of FY09. Our mission is to carry out a research program aimed at advancing the state of the art and development of magnet technology for fusion applications. This work is being carried out under funding from the Enabling Magnet Technology Program of the Virtual Laboratory for Technology (VLT). The Project is lead by Dr. Joseph V. Minervini (PI) and Dr. Makoto Takayasu (Co-PI). The work is being out in the research laboratories of the MIT Plasma Science and Fusion Center.

The objectives of the program are to perform basic research in superconductor and magnet technology which 1) provides understanding of present state-of-the-art superconductors and magnet systems, and 2) to investigate new directions in applied superconductivity and use these, as appropriate, to advance the state-of-the-art in fusion magnet technology towards future application to DEMO and other advanced magnetic confinement devices.

Although this MIT group has previously been involved in the design, analysis, magnet fabrication, and component R&D for ITER magnets since the inception of the ITER program in 1987, including CDA, EDA, and preparation for ITER (2003-2006) phases, our involvement in ITER Magnets has been completely eliminated since February 2008.

The focus of the D&T-01 tasks was thus shifted to basic studies of magnet technology issues. Although these results can sometimes be directly applied to the present design of the ITER magnets and conductors, they are primarily oriented towards development of magnet technologies anticipated to be used in fusion applications in addition to, or beyond ITER.

The studies performed here are intrinsically fundamental in nature, or in a very early technology development stage. We have selected technical topics that are well suited for study by an academic institution, but the solutions are always approached with a practical experience background of implementing new technology in working devices, and with an eye on eventual technology transfer to industry.

The program is focused into 6 subtasks:

1. ***VLT Enabling Technology Magnets Program***
2. ***Bending-Strain Effects of Critical Currents on Nb_3Sn Wires***
3. ***Transverse Stress Effects of Critical Currents on Nb_3Sn Cables***
4. ***High Temperature Superconductor Torsion Property of Critical Currents and New HTS Tape CICC***
5. ***Development of Quench Code Solxport3D-Quench***
6. ***Modeling of Cabling 3D Twisting Pattern***
7. ***Study of the Jacket Materials for CS Coils***

The program status and task details are described in the following sections of this report.

2 VLT ENABLING TECHNOLOGY MAGNETS PROGRAM

Since many years the Office of Fusion Energy Sciences has organized all enabling technology activities under a national structure called the Virtual Laboratory for Technology. Within that program Joseph Minervini has served as spokesperson for Magnet Technology since 1996. In that role, he interacts with the VLT leadership and responds to OFES request for programmatic guidance and input and annual budget requests. Also, in general, MIT serves as a national resource to the OFES program for support and guidance of SBIR programs and as a source of expert support for magnet engineering technology of various national fusion projects. MIT has also served the national program as a partner in bilateral and multilateral international projects and technology exchanges.

2.1 Personnel

There have been significant personnel changes within the Fusion Technology and Engineering Division this year relative to FY2008. The loss of US ITER funding in FY08 and limited base program funding in FY09 has resulted in a severe reduction of research staff in the Division. The entire Division was put on layoff notice last year. Although all of these people were not fully funded by the fusion program, they all had at some time, significant roles in fusion magnet technology, some of them having more than 25 years of experience.

Following is a list of long-term research staff who have left the Division and where they went:

1) Alex Zhukovsky (retired-reluctantly)
2) Philip Michael (transferred to LDX)
3) Chen-yu Gung (transferred to Alcator and later joined ITER IO)
4) Joel Schultz (Long term disability)
5) Valery Fishman (funded by non-fusion projects)
6) Walter Mann (laid off)
7) Barbara Keesler (laid off)
8) Peter Titus (Initially half time to Alcator and half time to GA. Now permanently employed at PPPL)
9) Bradford Smith (to industry)
10) Alexey Radovinsky (to industry)
11) David Tracey (technician- transferred to Alcator)

Other personnel changes include: Leslie Bromberg's long-time partial funding by the Advanced Design program was curtailed. He remains in the Division supported mostly by non-fusion funding, although recently part of his time has been subcontracted from PPPL to assist with magnets aspects of their program in advanced stellarator design.

Our Division and the Fusion Magnets Program suffered a major loss in January because Joel Schultz was afflicted with a serious medical condition. Fortunately, he is making a remarkable recovery. However, we lost his services from January forward. In July his employment at MIT terminated and he is now on long-term disability. We do however expect that at some time in the future, he might return to at least part-time employment. His deep experience and knowledge is very important to the fusion program.

With Joel's departure, we were able to retain Dr. Makoto Takayasu full-time. He has served as our chief laboratory scientist for more than 20 years. So we are fortunate that we can maintain at least a small experimental program.

2.2 Graduate Students

Last year (FY2008) the magnets base program supported three graduate students in their Ph.D. research. Scott Mahar received the Ph.D. in Nuclear Science and Engineering in September 2008. He is now employed at General Atomics, although he is in the Advanced Systems Division, not the Energy Division that supports DIII-D.

Luisa Chiesa received the Ph.D. in Nuclear Science and Engineering in November 2008. She is now an Assistant Professor of Mechanical Engineering at Tufts University. She is continuing here work in the field of applied superconductivity and we hope to able to collaborate with her in the future.

Matteo Salvetti is a Ph. D. candidate in the Mechanical Engineering Department. Since he has not yet concluded his thesis research, lack of funds required us to terminate his research assistantship after the Fall Term of 2008-2009 academic years. Fortunately he has continued his research with support from Prof. David Parks of Mechanical Engineering. Joseph Minervini remains on his thesis committee and we expect that Matteo will defend his thesis in the Fall Term of 2009-2010 academic year.

If funding for the Magnets Program remains at or below the present level, these will be the last students to have done their graduate research in the area of fusion magnet technology and applied superconductivity at MIT, closing a 30-year long chapter in education of students at MIT in this field.

2.3 Contributions Outside the Base Program

Jun Feng is now being engaged partially by PPPL to assist in materials aspects of the ELM and VS coils for ITER. He is applying his extensive knowledge of fracture mechanics and fatigue analysis to the conductors for these coils which must operate through thousands of plasma cycles and magnitudes more mechanical cycles.

As mentioned above, Leslie Bromberg is also partially supported by funding from PPPL to design and analyze a new concept for stellarator magnets by using High Temperature Superconducting (HTS) bulk 'tiles' to create complex 3D fields by their diamagnetism (flux exclusion) or through flux trapping.

Joseph Minervini served as a member of the OFES Committee of Visitors (CoV) this year. He is also participating as a magnet expert in the next meeting of the ITER STAC (STAC7).

2.4 ReNeW

We were very active in representing Magnets Technology throughout the fusion community's national program for the Research Needs Workshop (ReNeW). Joseph Minervini served as Magnets Panel leader. Other panel members included Prof. David Larbalestier (FSU), Dr. Richard Thome (GA), Dr. GianLuca Sabbi (LBNL), Dr. Bradley Nelson (ORNL-USIPO), Dr. Michael Gouge (ORNL-HTS), Leslie Bromberg (MIT), and Joel H. Schultz (MIT).

Although Joel Schultz's participation was very limited due to a sudden and long lasting medical condition, earlier white papers, reports and publications, he wrote, including those from Snowmass, provided a rich basis for structuring the final thrust.

Joseph Minervini very much appreciated the contributions from the other panel members, especially because they receive no funding from the fusion base program.

The Magnets Panel efforts were well worth the time because the ReNeW Final Report[1] contains a major thrust:

> **"Thrust 7: Exploit high-temperature superconductors and other magnet innovations to advance fusion research.** Magnets are crucial for all MFE concepts. This focused Thrust would perform the research necessary to enable revolutionary new high-temperature superconducting materials to be used in fusion applications. Key activities include development of high-current conductors and cables, and integration into components of fusion research experiments, with great potential to improve their design options."

OFES is presently considering the next steps with regard to the ReNeW recommendations, and we remain ready to implement any new directions authorized by the Office. In the meantime, the present program tasks described here are already in synchronism with the spirit of Thrust 7.

3 BENDING-STRAIN EFFECTS OF CRITICAL CURRENTS ON NB3SN WIRES

Summary
Mechanical load effects of Nb_3Sn conductors have been studied with focusing on bending strain effects of strands and transverse load effects of CICC cables, in order to understand the

[1] Report of the Research Needs Workshop (ReNeW), Bethesda, Maryland – June 8-12, 2009

critical current degradations of large-scale cable-in-conduit conductor (CICC) magnets that are exposed to significant Lorentz forces. These research studies have been carried out primarily as graduate student thesis work. In 2009 significant progress has been made in both areas, and the primary goals have been completed. Even still there are important research areas remaining to be investigated. One of the graduate students, Luisa Chiesa has taken a faculty position at Tufts University, Medford, MA near MIT. She is organizing her Lab to continue superconducting conductor researches for Fusion including the extension of the research on bending and transverse-load effects. We expect to collaborate with her and her students on those subjects. We have also started a new area of investigation for application of HTS 2G conductors for fusion magnets.

3.1 Introduction

The effects of bending on the critical current behavior of a superconducting strand were investigated to understand the operation current degradation of large Nb_3Sn superconducting cables. Bending phenomena of Nb_3Sn wires were experimentally characterized using a previously reported variable pure-bending strand test device [3.1]. The critical currents were measured over a wide range of bending, up to the nominal bending strain of 0.8% at the outer strand surface. Five different Nb_3Sn wires developed by the ITER parties were evaluated. Irreversible degradation of the critical currents due to bending was also evaluated. An integrated model has been developed for a Nb_3Sn wire taking into account the neutral axis shift, the current transfer length, the mechanical filament breakage, and the uniaxial strain release due to applying bending. The experimental data were analyzed with a newly developed integrated model using the existing uniaxial strain data of the wires. The current transfer effect appears to be an important factor. This work was presented at the CEC-ICMC 2009 and summarized in a publication [3.2].

3.2 Model

The critical current of a multi-filamentary twisted superconducting strand under bending strains has been formulated by Ekin [3.3], and his concept has been adopted for various studies [3.4]-[3.7]. Ekin considered critical current transfer between filaments due to axial strains under bending in a twisted strand. Two extreme cases have been considered: long twist pitch (low inter-filament resistivity), and short twist pitch (high inter-filament resistivity). We will call the former case "Perfect Current Transfer," and the latter "No Current Transfer."

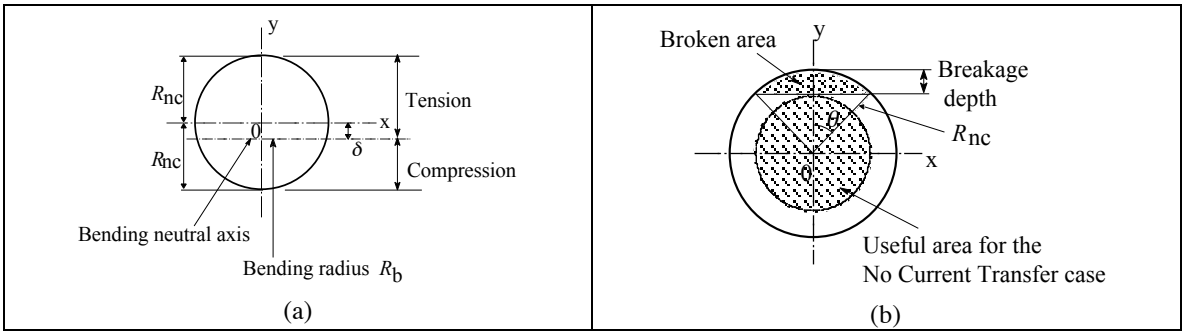

Fig. 3.1 (a) Cross-section of non-copper showing the neutral axis shift of δ, and (b) schematic of non-copper area having broken filament area.

In general, the experimental results of the critical currents under a wide range of bending strains have been known to fit neither the Perfect Current Transfer model nor the No Current Transfer model. Our experimental results show only a good fit to the Perfect Current Transfer model at small bending rates and then sharply dropping off toward the prediction line of No Current Transfer model with increasing bending. We have investigated four effects due to mechanical bending: the neutral-axis shift [3.3], [3.8], [3.9], the current transfer length, the filament breakage [3.10], and the uniaxial strain releasing [3.8], [3.11]. Fig. 3.1 shows the strand cross-section views to illustrate the neutral-axis shift model (a) and the filament breakage model (b).

Neutral-Axis Shift Effect:

A shift of the neutral-axis due to yielding of the strand matrix under bending has been pointed out by Ekin [3.3]. The neutral-axis shifts toward the compressive side by δ as shown in Fig. 3.1a. Fig. 3.2 shows the calculated neutral-axis shift effects on the critical current for the Perfect Current Transfer and No Current Transfer cases, respectively. In the Perfect Current Transfer case the critical current shows a maximum peak at certain conditions since the tension area increases. This was observed for the Furukawa wire (Fig. 3.5e).

Current Transfer Length Effect:

The current transfer length affects the total critical current with regard to the twist pitch length L_p. The current transfer length L_{ct} has been given as a function of the transverse resistance of matrix material between filaments and the n-value of the resistive transition of the superconductor by [3.6], [3.12], [3.13]. Regardless of the accuracy of the current transfer length itself, the relative ratio of the current transfer length to the twist pitch (L_{ct} / L_p) is an important factor for characterizing the current transfer effects on the critical current. To take into account the current transfer effect, the critical current of a filament at a given point z along a filament is assumed to be dominated by the minimum critical-current value between z - L_{ct}/2 and z + L_{ct}/2.

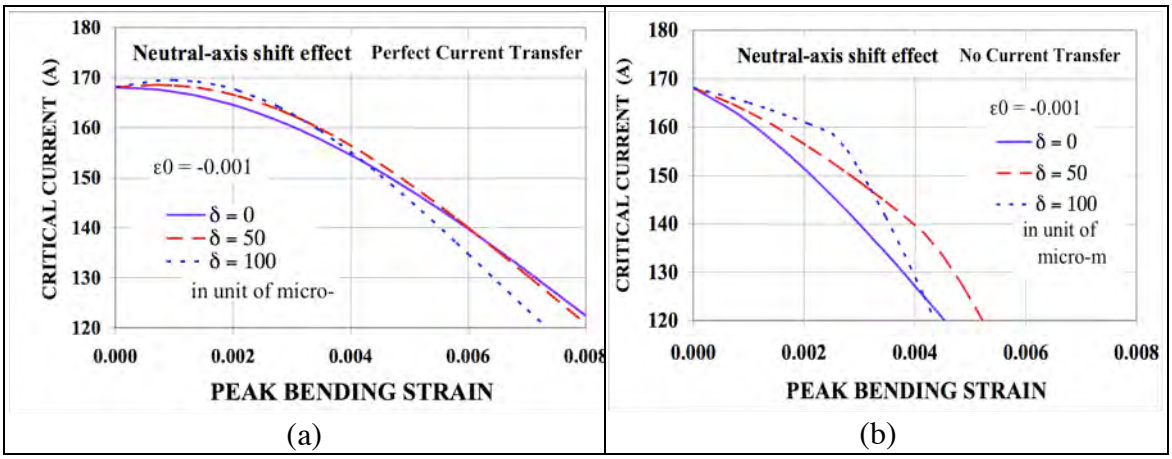

Fig. 3.2 (a) Calculated critical currents of neutral-axis shift effect for Perfect Current Transfer, and (b) calculated critical currents of neutral-axis shift effect for No Current Transfer.

Fig. 3.3 shows the calculated critical currents with various current transfer lengths L_{ct} of 0.5 mm, 1 mm, 2.5 mm and 5 mm for a strand with the twist pitch L_p = 10 mm. These L_{ct} values

correspond to 0, 5%, 10%, 25% and 50% of the twist pitch length. The curves of L_{ct} = 0 and L_{ct} = 0.5 L_p agree with the results of Perfect Current Transfer (open circle) and No Current Transfer (open triangle), respectively.

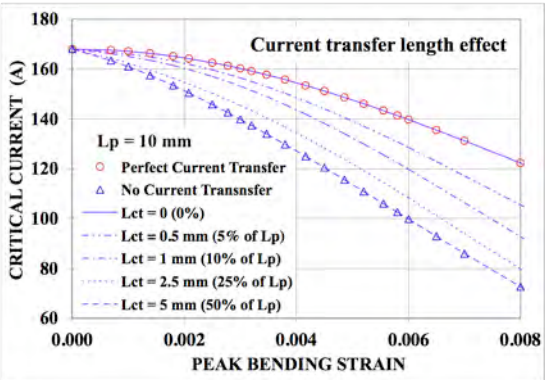

Fig. 3.3 Calculated critical currents of current transfer effect with various current transfer lengths.

Filament Breakage Effect:

Filament breakages in the tension side due to bending have been found [3.10]. Such filament breakage is probably the dominant cause of the irreversible permanent degradation. If the filament breakage occurs near the surface of the tension side as shown in Fig. 1b, the critical currents can be obtained with integration over the unbroken area for the Perfect Current Transfer case. However, in the case of No Current Transfer, the effective superconducting filaments are only in the center circular section, which does not overlap the broken area since the strand is twisted.

Fig. 3.4a shows the calculated critical currents of the filament breakage for the Perfect Current Transfer (dotted lines) and No Current Transfer (bold lines) cases with the breakage area fractions of 0%, 2% and 5%. In the case of Perfect Current Transfer, critical current degradations are the same rates as that of the breakages. On the other hand, the degradations of the No Current Transfer case are significant, for example, about 35% for the 5% breakage even at zero bending (Fig. 3.4b).

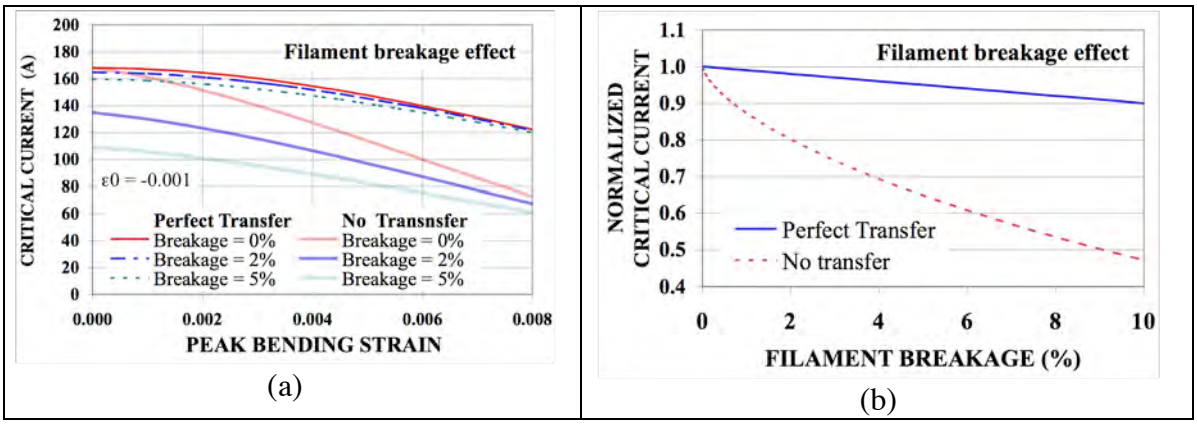

Fig.3.4 Calculated critical currents of the filament breakage effect of Perfect Current Transfer (dotted lines) and No Current Transfer (bold lines) cases for the breakage fractions of 0%, 2% and 5% (a). Critical current degradations due to the breakage at zero bending for Perfect Current Transfer and No Current Transfer (b).

Uniaxial Strain Releasing Effect:
Uniaxial thermally induced precompressive strain during cooldown after reaction of a Nb_3Sn wire could be released by mechanical bending cycles [3.11]. The result is that the strain $|\varepsilon_{max}|$ becomes smaller, and the critical current increases. The increase of the critical current at zero bending after bending cycles could be driven only by this strain releasing effect. In the present experiments, this effect seemed to be very small, but did appear for some wires.

3.3 Analyses of Experimental Results

The bending tests were carried out in 2008 using our variable bending test device developed and described earlier [3.1]. The device can apply a large range of bending, in liquid helium, to a strand sample of about 100 mm length, up to 0.8% of the nominal bending strain at the surface of a wire of 0.8 mm diameter.

We investigated five different Nb_3Sn wires which were developed by the ITER parties. Three were internal-tin wires of recently developed ITER TF US Oxford and Luvata wires and EU EM-LMI wire. Two of them were bronze wires of EU European Advanced Superconductors (EAS) and Japanese Furukawa designs, developed during the ITER Engineering Design Activity of the 1990's. Test wire characteristics and their heat-treatment schedules are shown as well as details of experimental results in [3.14]. The bending tests were performed at 12 T or 15 T in liquid helium using the 20 T, 195 mm Bitter magnet at NHMFL, Florida State University. The test results are shown in the following section.

To use the scaling law of the critical current equation commonly used [3.15] for analyses of the experimental results, parameters required for the equation were selected on the bases of various published work [3.5], [3.16]-[3.18]. A few parameters for the wires presented in this work were not available, so they were adjusted by our measured critical current results of magnetic field dependences. The parameters used for the tested wires are summarized in Table 3.1. The parameters of p and q were p=0.5 and q=2. These parameters might not be accurate, however, the results of the model analyses are not strongly affected by modest changes of the parameters.

Table 3.1 Scaling parameters in equation 1 used for tested wires.

Strand	Oxford	Luvata	EAS	EM-LMI	Furukawa
B^*_{c20max} (T)	32.5	32.5	35.75	28.7	32.5
T^*_{c0max} (K)	17.8	17.0	16.52	16.89	16.5
C (AT)	18500	17000	14150	12750	11500
ε_{0a}	0.00344	0.0034	0.0025	0.0019	0.0020
ε_{max}	0.0005	0.0011	0.0024	0.0011	0.0023
C_{a1}	53.3	60.0	71.39	45.16	44.35
C_{a2}	8.55	20.0	28.28	8.45	12.25

The critical current behavior of each wire tested for bending strains was unique as shown below. The critical current trends with the bending strains were analyzed by selecting the best fitting parameters of the four effects using a curve fitting method.

Curve fitting results for the Oxford sample are shown in Fig. 3.5a. Experimental results are shown with solid circles as a function of the peak bending strain of the filament which is the maximum bending at the outermost filaments. The measured data lie between curves obtained from the Perfect Current Transfer model (upper thin line) and the No Current Transfer model (lower thin line). The bold line was obtained by taking into account the four effects: the neutral axis shift, the current transfer length, the filament breakage and the uniaxial strain releasing, in order to fit the experimental data. Details of their parameters of the four effects used for the fittings are found in [3.2]. Three dotted lines in Fig. 3.5a show calculated recovery curves of the critical currents after the peak bendings of 0.42%, 0.49% and 0.56%, respectively. The recovered critical currents at zero bending agree well with the experimental results. The Oxford wire sample showed significant irreversible permanent degradation, which could be explained with 2% filament breakage at 0.56% of the peak bending strain.

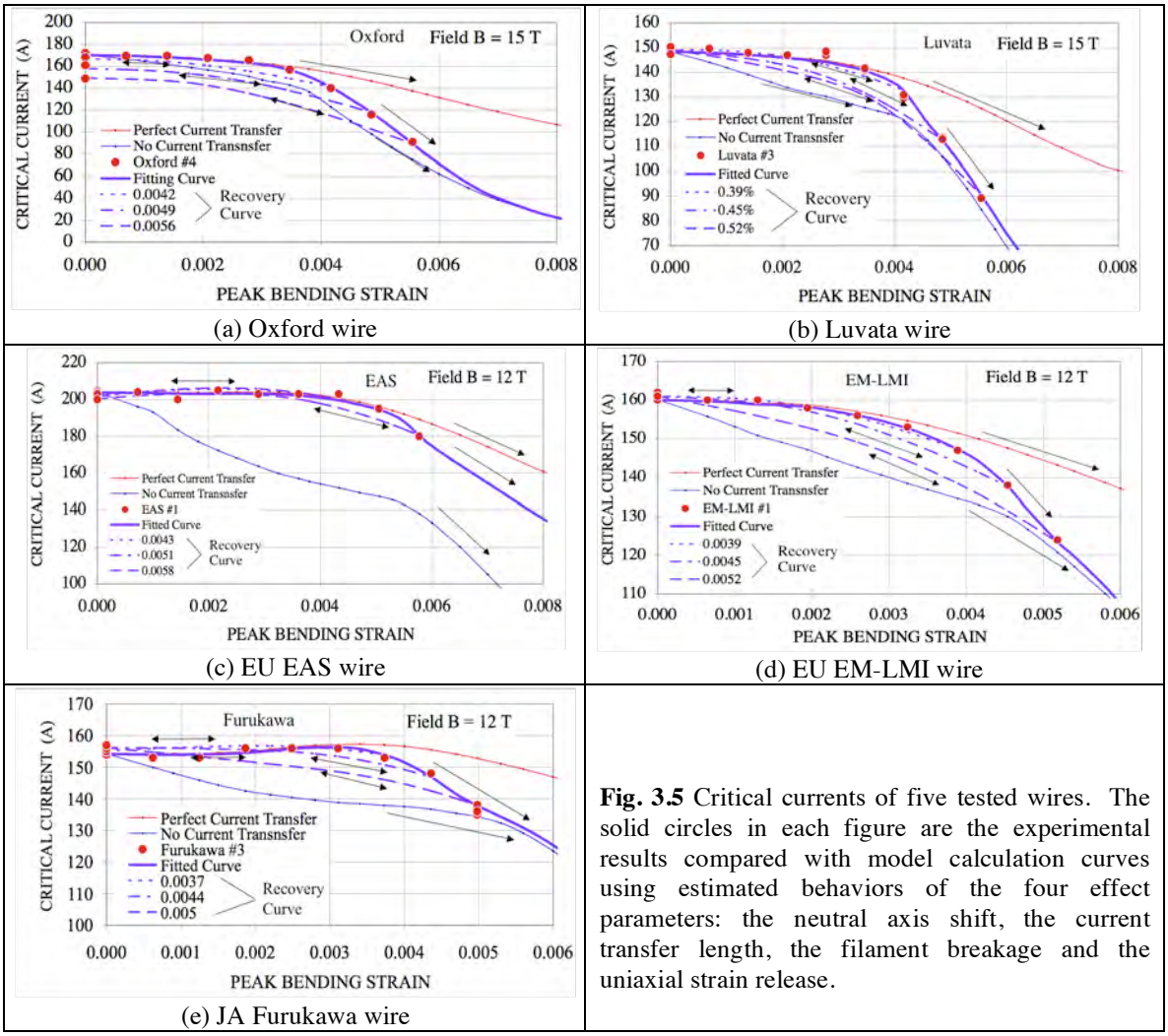

Fig. 3.5 Critical currents of five tested wires. The solid circles in each figure are the experimental results compared with model calculation curves using estimated behaviors of the four effect parameters: the neutral axis shift, the current transfer length, the filament breakage and the uniaxial strain release.

Fig. 3.5b shows the curve fitting results of a Luvata wire sample. The sharp decrease of the critical current above 0.45% bandings was reflected by the sharp increase of the current transfer length. Permanent degradation of the Luvata sample was negligible, implying an

absence of filament breakage. Fig. 3.5c shows the curve fitting results of an EU EAS wire sample. The EAS wire sample showed very small bending effects. The critical current increases slightly with increasing bending strains. This probably is the result of neutral axis shifts. Fig. 3.5d shows the curve fitting results of an EU EM-LMI wire sample. The internal tin EM-LMI sample showed bending effects as large as other internal tin wires of Oxford and Luvata wires. Permanent degradation of this wire was small, similar to the Luvata wire. Fig. 3.5e shows the curve fitting results of a Furukawa wire sample. The 1% increase of the critical current for the Furukawa wire sample at 0.3% peak bending can be simulated by assuming a 70 μm shift of the neutral axis. Three dotted lines show recovery curves of the critical currents after the given bendings of 0.37%, 0.44% and 0.50%. The maximum of the critical currents at about 0.3% peak bending and also the recovered critical currents at zero bending both agree well with the experimental results.

3.4 Conclusions

The critical currents of the internal tin wires were degraded by 47% for Oxford wire, 40% for Luvata wire at the 0.56% peak bending strain, and 30% for EM-LMI wires at the 0.52% peak bending strain. Higher current density wire, such as the Oxford wire, seems to degrade more than the lower current density wires. On the other hand, bronze wires of EAS and Furukawa both degraded by only about 10%. After about 0.5% peak bending, Oxford, Luvata and ESA wires showed 13%, 1.3% and 2% irreversible permanent degradation of their initial critical current values, respectively. However, the critical currents of EM-LMI and Furukawa wires increased slightly gradually at zero bending strain after each bending cycle. It was found that the Furukawa wire showed clear improvements of the critical currents at the peak bending of around 0.3%.

The experimental behavior of the critical currents for a Nb_3Sn strand due to pure bending has been evaluated using the four effects: the neutral axis shift, the current transfer length, the filament breakage and the uniaxial strain release. The neutral axis shift increases the critical current under small bending strains (~0.3%), but does not change the critical current at zero bending state. The current transfer length reduces the critical current with increasing ratio of the current transfer length and the twist pitch length. The current transfer length effect seems to be an important factor, which is a function of the n-value of the superconductor and the transverse resistance of the matrix. A strand having a longer twist pitch has a smaller effect due to the current transfer length. Longer strand twist pitch is desired, although it is typically harmful for AC coupling losses. The filament breakage reflects an irreversible permanent degradation. The filament breakage could result in significant degradation for a strand having a long current transfer length (short twist pitch). The uniaxial strain release (reduction of thermally induced strain) causes enhancement of the critical current.

Further investigations of the mechanical dynamics of the superconducting matrixes during bending are recommended. The recovery behavior of the critical currents after applying bending is very useful to understanding the effects of bending on the critical currents.

3.5 References

3.1 Harris, D.L. et al., *Adv. Cryo. Eng*., **54**, Plenum, N.Y., 2008, pp. 341-348.
3.2 M. Takayasu, et al., presented at CEC-ICMC 2009, accepted for publication of *Adv. Cryo. Eng*.
3.3 Ekin, J.W., Proceedings of the tropical conference on A15 superconductors, Ed by M. Suenaga and A. Clark, Plenum Press, New York, 1980, pp. 187-203.
3.4 Mitchell, N., *Cryogenics*, **43**, 2003, pp. 255-270.
3.5 Nijhuis, A. and Ilyin, Y. , *Supercon. Sci. Technol.* **19**, 2006, pp. 945-962.
3.6 Nijhuis, A. et al., *Supercon. Sci. Technol*. **19**, 2006, pp. 1136-1145.
3.7 Koizumi, N. et al., *IEEE Trans. Appl. Supercond*. **16**, 2006, pp. 831-834.
3.8 Kaiho, K., et al., *Appl. Phys. Lett*. **36**, 1980, pp. 223-225.
3.9 Kubo, Y. and Ozawa, T., *Journal of the Cryogenic Society of Japan*, **37**, 2002, pp. 68-76.
3.10 Jewell, M.C. et al., *Supercond Sci Technol*, **16**, 2003, pp. 1005-1011.
3.11 Miyoshi, K. et al., *Adv. Cryo. Eng*., **52**, Plenum, N.Y., 2006, pp. 536-543.
3.12 Ekin, J. *J. Appl. phys*. **49**, 1978, pp. 3406-3409.
3.13 Ekin, J. and Clark, A.F., *J. Appl. phys*. **49**, 1978, pp. 3410-3412.
3.14 Takayasu, M. et al., MIT Plasma Science and Fusion Center Report, PSFC/JA-08-41, 2008.
3.15 Bottura, L. et al., CERN-ITER collaboration report, Version 2, April 2008.
3.16 Nijhuis, A., *Supercond Sci Technol*, **21**, 2008, pp. 1-15.
3.17 Ilyin, Y. et al., *Supercond. Sci. Technol*. **20**, 2007, pp. 186–191.
3.18 Taylor, D.M.J. and Hampshire, D.P., *Supercond. Sci. Technol*. **18**, 2005, pp. S241–S252.

4 TRANSVERSE-STRESS EFFECTS OF CRITICAL CURRENTS ON NB3SN CABLES

4.1 Introduction

The electromagnetic interaction between current and magnetic flux in a cable-in-conduit conductor (CICC) results in a significant Lorentz force accumulating across the cross section of the conductor. This transverse load is one of the causes of the unexpected degradations seen in large CICC magnets such as the ITER model coil magnets [4.1].

Our experimental work of the transverse load effect on superconducting cables has been completed in 2008. In FY2009 the study was continued for experimental data analyses and new model developments to understand the transverse load effects on a CICC cable.

A new model based on contact mechanics concepts has been developed to analyze and quantitatively evaluate mechanical transverse load effects on superconducting strands in a cable-in-conduit-conductor (CICC). It has been used to determine the number of contact points and the effective contact pressures among the strands in a cable. The new model has been confirmed by experimental measurements and it is used to explain mechanical transverse load effects on the critical current degradation of sub-sized cable samples.

Based on the present model, we have proposed an evaluation method of the transverse load effects of a full size CICC cable. It will allow prediction of the transverse load degradation of a CICC cable made from newly developed wires.

This work was presented at the CEC-ICMC 2009 [4.2] - [4.3].

4.2 Model Concept of Transverse Load Effect on CICC Cables

The number of strand-to-strand contacts is calculated for the different stages starting from a 3-strand cable. In general a cable-in-conduit conductor is produced in multiple stages starting from twisting three strands (triplet) together and then twisting together three or four bundles and so on, until the final stage is reached. When a transverse load is applied to a 3-strand cable it is noted that there are six places of strand-to-strand contact points that support the load in one twist pitch length as shown in Fig. 4.1. At each contact, two strands overlap each other to make one strand-to-strand contact, so that the total number of strand-to-strand contacts is 6 per twist pitch, which is twice the number of strands composing the cable. The next stage could be composed of three, four or five bundles of 3-strand cables (3x3, 3x4, 3x5). In general, the contact places between sub-bundles are given by $2 \cdot k$ where k is the number of bundles. The distribution of the strand-strand contact points in a cable is determined by extension of this contact point analysis [4.3].

Evaluation of the transverse load effect on the critical current of one strand composing a cable is based upon evaluation of the contact pressure p_{cy} of the strand at each strand-strand contact point. This pressure is given by the ratio of the contact force F_{cy} on a strand at a particular location, divided by the contact area S_c ($p_{cy}=F_{cy}/S_c$) obtained from contact mechanics [4.4] - [4.6]. The contact force F_{cy} is the ratio of the force acting on a layer divided by the contact points in the layer ($F_{cy}=F_{LFy}/N_{hy}$). Once we know the contact point distribution in a cable as mentioned above, the contact force and the contact area can be calculated.

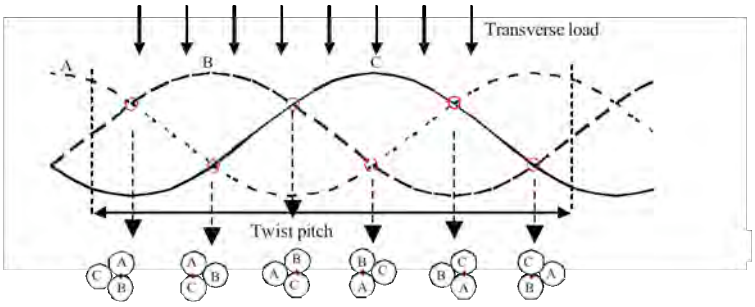

Fig. 4.1 Cross contact places of a 3-strand cable under transverse load in one twist pitch length.

It is noted that the Young's modulus E is the only unknown parameter in this model calculation, and it is obtained experimentally from the cable displacement measurement during transverse load tests. Fig. 4.2 shows the calculated displacement compared with the experimentally measured one [4.2] for the 3-strand cable. A fair agreement is obtained for values of E of 3 GPa. The values of the transverse Young's modulus found for those samples

are similar to the values reported in the literature [4.7]. The transverse Young's moduli are much lower than the values of solid metals composing the Nb_3Sn strands.

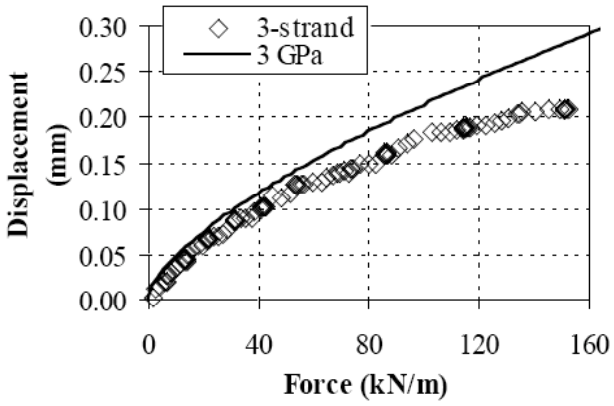

Fig. 4.2 Transverse displacement (measured and calculated) as a function of force per unit length for the 3-strand sample. Calculated curve is for E = 3 GPa. Critical current as a function of contact pressure obtained with E = 3 GPa.

4.3 Modeling of Critical Current Behaviors

Transverse loads are caused by an external mechanical load or an electromagnetic Lorentz load due to the self current and total magnetic field. There is a fundamental difference between these two approaches. The external mechanical load is applied uniformly through the cross section of a cable, while the Lorentz load is caused by a body-force which accumulates through the cross section. The model takes into account these two different scenarios to evaluate transverse load effects on the critical current in a cable. The critical current of a strand is evaluated as a function of the contact pressure.

In the case of the external mechanical load, the force in each horizontal plane is the same. Each strand in a horizontal plane experiences the same contact force (the transverse load divided by the number of contacts in a plane perpendicular to the load).

Fig. 4.3 shows the experimental results of the 3-strand cable as a function of the effective contact pressure due to the external load. The pressure was evaluated from the model analysis. The solid line in Fig. 4.3 was obtained as the best fit with a fitting parameter for the Young's modulus of E = 3 GPa. This fitting curve was then used to estimate the behavior of larger cables.

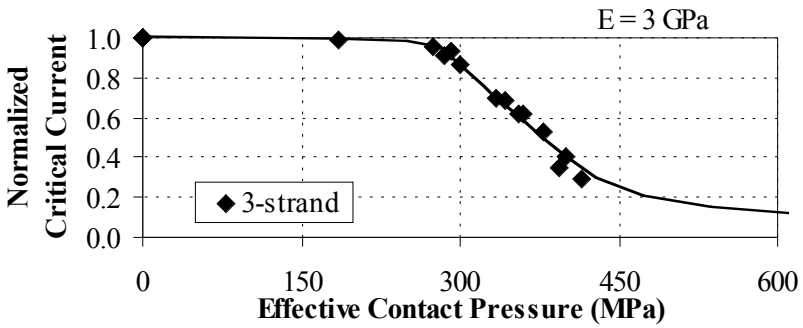

Fig. 4.3 Three-strand cable data and fitting curve used to predict the behavior of the 45-strand sample.

Fig. 4.4 shows the 45-strand experimental data and the two theoretical curves determined from the twisted and untwisted cable models using the 3-strand fitted curve shown in Fig. 4.3. The experimental data are between the two lines obtained from the twisted and untwisted cable models. Since the pressed test section length of the sample was similar to the last stage twist pitch, the 45-strand cable could not be considered to be fully twisted. The experimental data are well matched by the model curves.

Those results are very encouraging because they suggest that experimental results of the smallest stage of a CICC could be used to estimate the behavior of a larger size cable subjected to a certain transverse loads thus voiding expensive experiments on large CICC.

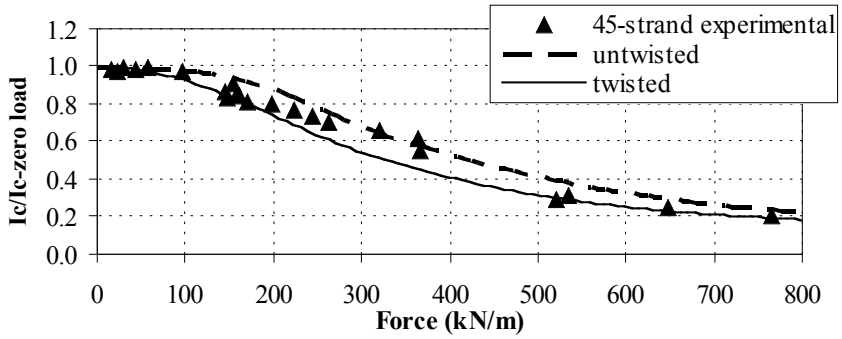

Fig. 4.4 Normalized critical current as a function of force per unit length of the 45-strand sample and the calculated curves obtained from the model.

In the case of the Lorentz load without the external force, the contact force between strands due to the Lorentz force will depend on the location of the strand in the cable since the forces accumulate along the Lorentz force direction. From the calculated contact pressure, the critical current of each strand can be obtained as a function of the contact pressure by using the 3-strand experimental results. The total critical current of the cable as a function of load can be obtained for both an untwisted and fully twisted cable with a summation of the all strand currents in a cable by a computer integration method.

In the case of a fully twisted cable each strand is assumed to spiral along the cable axis, and in a twist pitch length it will go back to its original location. In a twist pitch length, each

strand will experience the highest Lorentz load at some point so that the currents of strands on the same annulus will transport the same current corresponding to the minimum critical current experienced in a twist pitch length. No current sharing among strands is assumed in a twist pitch length.

4.4 Model Results

In order to perform the analyses we require knowledge of the critical current behavior of a strand under transverse pressure for a given wire, as discussed above. In the following analyses we use the experimental data obtained at the background field of 12 T for the 3-strand sub-cable experiment of Oxford ITER pre-production Nb_3Sn wire, and we use 3 GPa for the Young's modulus. The purpose of the model analyses is to have a general idea of the effects of the transverse load. The model results show that for a full size cable with the original cable pattern proposed for the TF coil in ITER (cabling pattern 3x4x4x4x6 and twist pitches 65, 90, 150, 270, 430 mm), the Lorentz load could account for up to 20% of degradation as shown in Fig. 4.5. Cabling patterns and twist-pitches of cabling mitigate the effect of the transverse load as shown in Fig. 4.6. Lower number of bundles in a stage causes higher degradation in general. A cabling pattern 3x3x3x3x6 shows a 10% larger degradation than a cabling pattern 3x5x5x6 (Fig. 4.6a). Shorter twist pitches at the first stage are preferable (Fig. 4.6b).

Tests performed on full size magnets (TFMC, TFI, CSMC, CSI) showed unexpected initial degradation (50% TFMC, 35% CSI, TFI, 25% CSMC) [4.1]. Our model shows that the Lorentz load effect is one significant player in the degradation, showing 30% degradation at operational current of 80 kA for the TFMC.

It is noted that the model presented here takes into account only the degradation caused by the transverse contact pressure due to the Lorentz load. Axial and bending strains caused by thermal contractions and by the Lorentz load could explain the additional sources of the degradation, and can affect the performance of superconducting strands and of a full size cable, as discussed in [4.8] – [4.10]. Those effects are complementary and not mutually exclusive, so all should be accounted for in prediction of the overall performance of a cable.

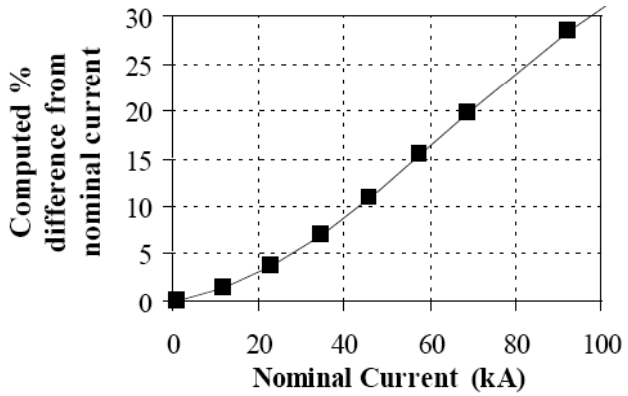

Fig. 4.5 Percent differences between the nominal current and the expected values considering the natural Lorentz load effect for the proposed TF cable configuration 3x4x4x4x6.

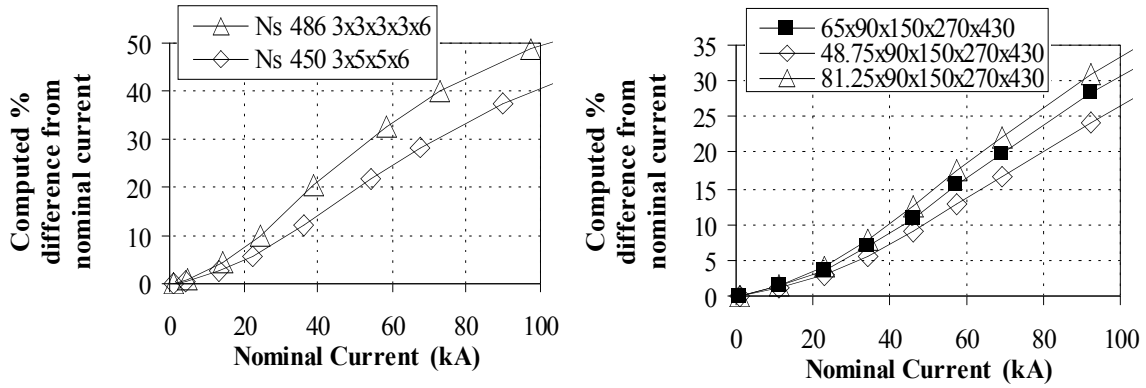

(a) (b)

Fig. 4.6 Percent differences between the nominal current and the expected values considering the Lorentz load effect for a cable with different cabling pattern (a) and twist pitch configurations (b).

4.5 Conclusions

The smallest stage of a 3-strand cable could be tested and used to predict behaviors of a large CICC cable. Testing such a small cable can minimize test expenses, yet still provide sufficient data to appropriately assess the overall performance of large magnets.

More tests, using different types of strands and cable configurations, are necessary to improve the understandings of the contact pressure between strands and its effect on the cable performance. A more systematic approach to characterize the mechanical properties of superconductors should also be developed to fully understand the CICC cable performances.

A new model based on contact mechanics between strands was presented to explain the transverse load degradation. A method evaluating quantitatively the number of contacts and the effective contact pressure between strands has been developed. Using experimental data and our developed model, we propose to use the 3-strand transverse-load performance data of the critical current to simulate the degradation of a large full size cable due to Lorentz load effect.

The model predicts the critical current degradations of cables like an ITER full size conductor as high as 20% caused solely by the transverse Lorentz load effect. For the first time the contact pressure Lorentz load effect is quantitatively evaluated to be a significant fraction of the inherent degradation of a large Nb_3Sn superconducting cable. To reduce the degradation caused by the transverse Lorentz load, one should use a higher number of bundles in a stage, shorter twist pitches, and sub-cables supports. Other sources of strain such as axial and bending strains need to be considered to determine the overall degradation of a cable. Our model needs further verification with more experimental work by using different cabling parameters (twist pitch, cable pattern, and wire diameter) to investigate how to improve and optimize a cable design.

4.6 References

4.1 N. Martovetsky, *Physica C* **401**, pp. 22–27 (2004).

4.2 L. Chiesa, et al., presented at CEC-ICMC 2009, accepted for publication *Adv. Cryo. Eng.*
4.3 L. Chiesa, et al., presented at CEC-ICMC 2009, accepted for publication *Adv. Cryo. Eng.*
4.4 H. Hertz, "*Miscellaneous papers*", Macmillan and Co., New York 1896, pp. 313-327.
4.5 S.P. Timoshenko, J.N. Goodier, "*Theory of Elasticity*", 3rd ed., McGraw-Hill, NY, 1970, pp. 35-39.
4.6 K.L. Johnson, "*Contact Mechanics*", Cambridge University Press, Cambridge, UK, 1985, pp. 90-106.
4.7 A. Nijhuis et al., *IEEE Trans. Appl. Supercond.,* **14**, pp. 1489-1494 (2004).
4.8 N. Mitchell, *Fusion Engineering and Design*, Vol. **66–68**, pp. 971–993, 2003.
4.9 A. Nijhuis, *Supercond. Sci. Technol.* **21**, 054011, 2008.
4.10 Y. Zhai and M. Bird, *Supercond. Sci. Technol.* **21**, 115010, 2008.

5 HIGH TEMPERATURE SUPERCONDUCTOR TORSION PROPERTY OF CRITICAL CURRENTS AND NEW HTS TAPE CICC

5.1 Introduction

We have developed a new method to cable flat, HTS tapes in order to make high current conductors. We do this by first stacking flat tapes and then twisting them along the axis of the stack. This cabling method is conceptually different from the existing lapped (annular) type cabling method presently used for electric power applications. The method allows achievement of high current, compact conductors for high field fusion magnet applications.

We desire to understand the mechanical properties of HTS tapes, especially torsional strain phenomena, in order to determine fabrication degradations for HTS flat tape cablings, and also to develop better cable processing methods. Data from torsion studies of HTS tapes are very limited [5.1] – [5.3]. Here we develop analytical models of the torsion twist strains for an HTS tape, including those for tapes in both conventional lapped-tape and newly developed stacked-tape cables. The calculated torsional strains are correlated to the corresponding axial strains of the tapes. The model results are compared with critical current measurements of twisted BSCCO and YBCO HTS tapes. Characterization of the critical currents under a wide range of torsional strains was carried out at 77 K to determine the critical current degradation due to these mechanical strains. Irreversible degradation of the critical current due to applied torsion was also evaluated, as well as the effect of torsion cycling.

A torsional twist strain effect on the critical current of a thin HTS tape has been found to be well described by a longitudinal strain model taking into account the internal shortening compressive strains accompanied with the tensile longitudinal strains due to a torsional twist. The critical current of a twisted tape is given by the integration of the critical current densities corresponding to the strain distribution over the tape cross-section using axial strain data of the tape. The model is supported by experimental results of YBCO and BSCCO-2223 tapes. It has also been found that torsional twisting effects on the critical currents of a tape composing of the conventional lapped-tape cable and the twisted stacked-tape cable are described by the same equation as that of a twisted single tape. This work was presented at the CEC-ICMC 2009 [5.4].

5.2 Critical Current Analysis of Twisted Tape

Fig. 5.1 shows schematic illustrations of a twisted single flat tape, a conventional lapped-tape cable, and a twisted stacked-tape cable. Fig. 1a shows a thin rectangular tape (width w and thickness t) of the length L is twisted along the center axis. Fig. 5.1b illustrates a conventional HTS cable composed of multiple tapes lapped circumferentially on a cylindrical surface. A novel conductor concept we developed is an assembled stack of HTS tapes as illustrated in Fig.5.1c. The stacked conductor is twisted about the longitudinal axis of the stack. During the cabling processes of the conventional lapped-tape and stacked-tape cables, the HTS tapes experience torsional twisting strains. The axial longitudinal strains in both cases shown in Figs. 1b and 1c are mathematically treated in the same way.

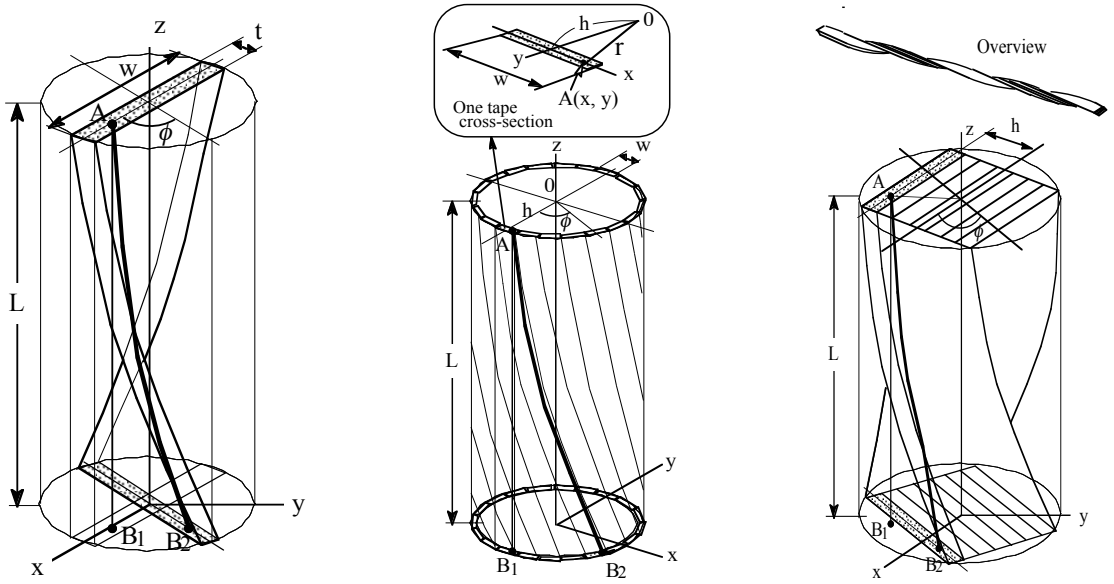

(a) (b) (c)

Fig. 5.1 Schematic illustrations of (a) a single twisted thin rectangular tape, and two types of HTS tape cables: (b) Conventional lapped-tape cable, and (c) Twisted stacked-tape cable.

It was found that the same torsional equation for a twisted single tape can describe the twisting effect on the critical currents of a tape composed by either the conventional lapped-tape cable, or the twisted stacked-tape cable. Furthermore, the actual longitudinal strain ε_x of each tape comprising the conventional lapped-tape cable and the twisted stacked-tape cable is equal to that of a twisted single-tape, and it does not depend on the tape location h in the y-direction. Therefore any tape in both lapped-tape and stacked-tape cables experience the exact same longitudinal strain distribution as that of the single twisted tape given by Eq. (5.1).

$$\varepsilon_x = \frac{\theta^2}{2}\left(x^2 - \frac{w^2}{12}\right). \tag{5.1}$$

where θ is the twist angle per unit length ($\theta = \phi / L$).

The critical current is a function of the axial longitudinal strain. Since the longitudinal

strains are not constant, but distributed, in a twisted tape, the critical current I_c of a twisted tape is written by a summation of critical current densities $j_c(\varepsilon_x)$ over the tape cross-section of the width w and the thickness t_s, corresponding to the strain distribution given by Eq. (5.1);

$$I_c = t_s \int_{-\frac{w}{2}}^{\frac{w}{2}} j_c(\varepsilon_x)\, dx . \tag{5.2}$$

The critical current density $j_c(\varepsilon)$ for an axial strain ε is obtained from critical current data $I_c(\varepsilon)$ of axial strain tests; $j_c(\varepsilon) = I_c(\varepsilon)/(t_s w)$.

5.3 Torsional Twist Test Method

Fig. 5.2a shows a torsion device we designed and fabricated to test a 380 mm long HTS tape including 40 mm terminations at both ends to a copper lead. The 300 mm test-section had two sets of voltage taps. The voltage tap separations were 100 mm and 200 mm. The lower termination of the sample is fixed, while the upper termination was mounted on a rotatable rod which was connected to a turn counter to measure the rotation with a resolution of 1 degree. The insert in Fig. 5.2a shows a twisted sample with voltage tap wires. Torsion experiments were performed with YBCO and BSCCO-2223 tapes under varying torsion. Tests were performed in liquid nitrogen (77 K) in the absence of externally applied magnetic field. The YBCO tape was a 2G Type SCS 4050 on 50 μm nickel alloy (Hastelloy®) substrate with a surrounding copper stabilizer (made by SuperPower, Inc.). The tape width and thickness were 4.05 mm and 0.128 mm, respectively. The BSCCO tape was a PIT-processed Bi-2223 in a silver alloy matrix with a clad of 35 μm stainless steel reinforcement on both sides (made by American Superconductor Corp., AMSC). The tape width and thickness were 3.05 mm and 0.249 mm, respectively. The BSCCO samples were the same type used to fabricate the levitating coil of the Levitated Dipole Experiment (LDX) [5.5].

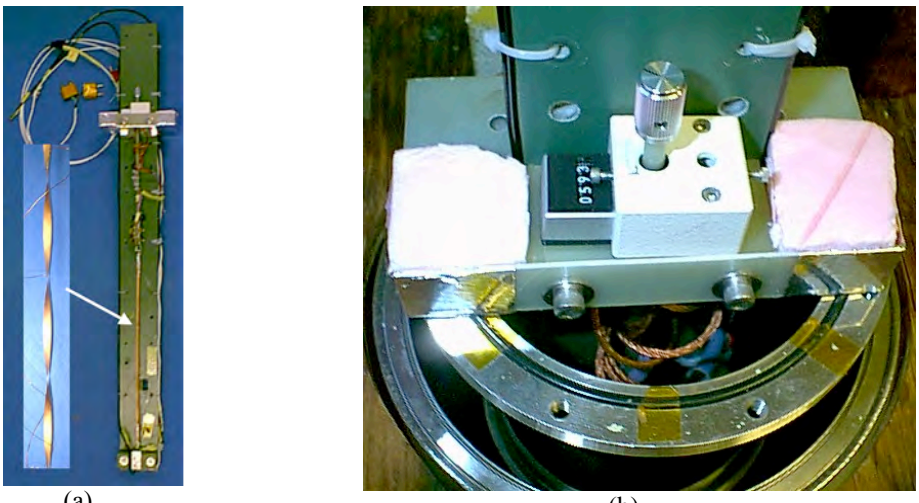

(a) (b)

Fig. 5.2 (a) Overview of a torsion test probe on a G10 plate of 915 mm height, 76 mm width and 6 mm thick. Test tape of a 300 mm section is twisted by rotating the upper current lead. The insert shows an enlarged twisted tape. (b) The probe is in a Dewar. A turn counter on a top flange measures the twisting angle.

5.4 Critical Current Torsion Test Results

Critical current test results of the YBCO sample for various torsions are shown in Fig. 5.3. The critical current normalized to the critical current of the undisturbed tape (86.5 A) is plotted as a function of the twist pitch in Fig. 5.3a. The voltage criterion used to determine the critical current was 100 μV/m. During application of the torsion (Torsion Up 1st cycle), the twist pitches was decreased to 100 mm, and then the twist pitches were increased to 1000 mm (Torsion Down 1st cycle). The normalized critical currents in the 1st cycle are plotted with solid and open circles in the figure. It is noted that the critical currents slightly increased with increasing torsion and then sharply decreased for twist pitches below 130 mm. The triangles in the figure shows the test results of 2nd cycle, where the twist pitches were decreased to 89 mm (Torsion UP 2nd cycle) and then the torsions were decreased to a twist pitch of 1000 mm (Torsion Down 2nd cycle). No permanent degradation of the current density was observed after the two-cycle processes. The n-values of the critical current ($V \propto I^n$), obtained at the criteria of 100 μV/m and 1000 μV/m, are shown in Fig. 3b. The n-values showed a tendency of decreasing very slightly during the two-cycle torsion process, but the n-values were ~32 consistently without significant torsion effects.

In Fig. 5.3a, the bold line shows an analytical behavior obtained with Eqs. (5.1) and (5.2) by using the published axial longitudinal strain data of SuperPower YBCO [13]. The integration in Eq. (5.2) was carried out by the Gaussian integration method of order 40 using Microsoft Excel®. The calculated curve, as shown in Fig. 5.3a, agreed very well with the experimental results. The critical currents increased by torsion above the twist pitch of about 150 mm may be due to the residual strain released by the torsional twist. The residual strain releasing effect was not included in the present analysis.

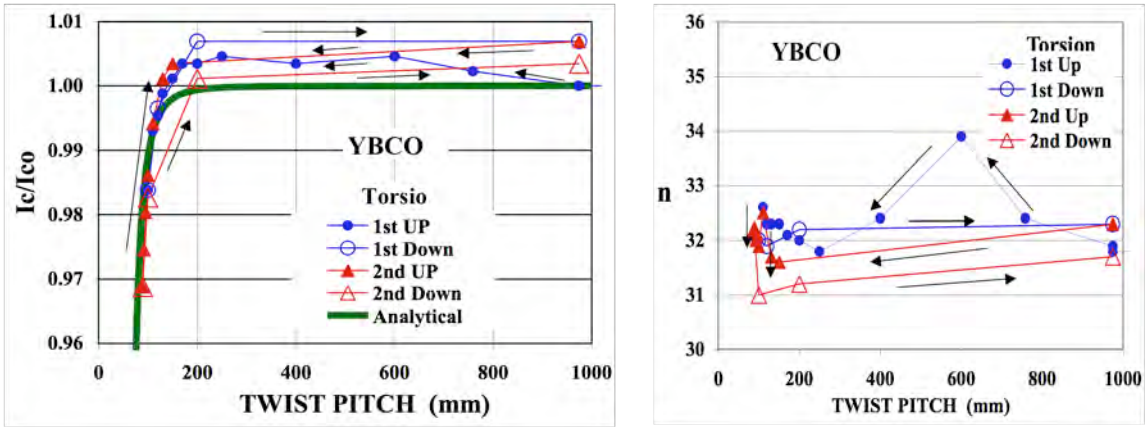

(a) (b)

Fig. 5.3. Critical current test results of YBCO obtained under various torsional twists; (a) The normalized critical currents with a curve calculated with the analytical mode, and (b) The n-values.

Test results of BSCCO-2223 tapes are shown in Fig. 5.4. The critical currents normalized to the initial critical current of the undisturbed tape (69.4 A for the 1st sample and 67.4 A for the 2nd sample) are plotted as a function of the twist pitch in Fig. 5.4a. Two samples obtained from the same spool were tested. During the application of the torsion, the torsion of one sample (open circles) was released once at a twist pitch of 103 mm, while for the other

sample (crosses) it was released 9 times as shown in the figure. The data clearly showed that the degradations due to the twisting did not recover after the torsion strains were released. The torsion or strain seems to create permanent damage. Fig. 4 shows the degradation of the critical current sharply increased for twist pitches shorter than 200 mm. A bold line in Fig. 5.4 shows an analytical result obtained from Eqs. (5.1) and (5.2). In the analysis the critical currents of the BSCCO as a function of the axial strain were approximated by axial longitudinal strain data which were selected to reflect the manufacturer's general specification values of 5% degradation at 0.4% strain for the BSCCO-2223 tapes.

The experimental results depart sharply from the analytical line below the twist pitch of 200 mm as shown in Fig. 5.4. The plastic yielding of the tape was not considered in the analytical model, however, the tested tapes clearly showed permanent twisted-deformation when the applied torsion was released. As mentioned earlier, the maximum shear stress occurs at the tape center surface. Therefore, the center area of the tape, where strain is compressive, could be yielded more than other areas of the tensile strain. Consequently the actual compressive strain could be larger than the calculated values, and therefore, one can expect that the critical current degradation rapidly increases with twist pitch below 200 mm, corresponding to the yielding phenomena.

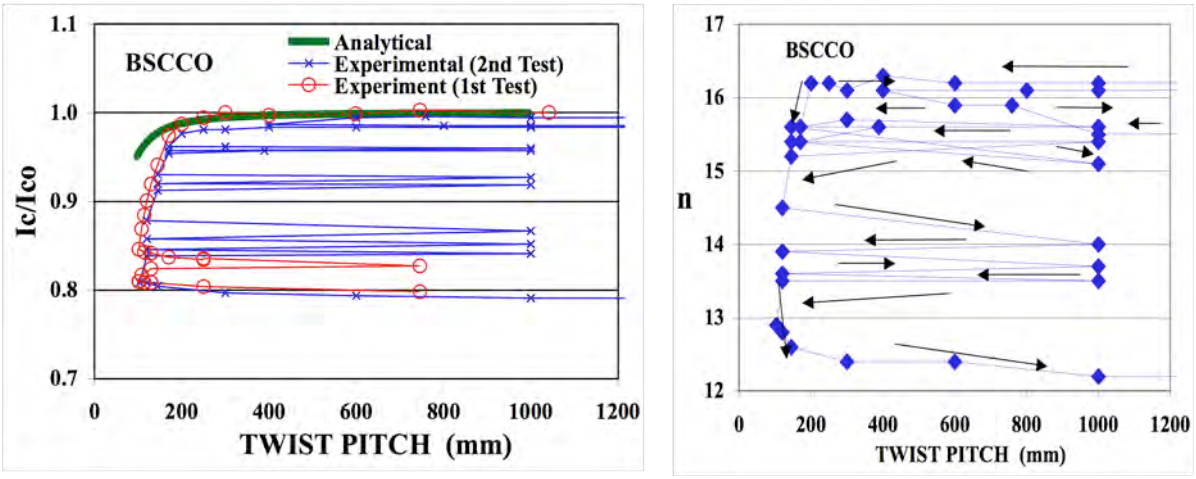

(a) (b)

Fig. 5.4 (a) Normalized critical currents as a function of the twist pitch. Two BSCCO tape tests are shown along with a curve of the analytical model. (b) The n-values of the 2nd sample.

5.5 Discussion

The critical currents of YBCO tape of the 4 mm width were not degraded by twisting of up to a 200 mm twist-pitch. Below 130 mm twist-pitch the critical currents degraded very sharply as seen in Fig. 5.3. At 90 mm twist-pitch the critical current degraded by 3%, but no permanent degradation was observed when the twist was released. The theoretical curve obtained from Eq. (5.2) in Fig. 5.3a agreed very well with the experimental results. On the other hand, the critical currents of BSCCO tapes of 3 mm width with a 35 μm stainless steel reinforcement on the both sides were degraded at 200 mm twist-pitch by about 2%, and then sharply degraded with increasing twist pitch. For a 120 mm twist pitch, the critical current

degraded by 20%. The degradation of the BSCCO-2223 tape due to the torsion was not recovered after removing of the torsion. We conclude that 2G YBCO tapes are very strong to mechanical twists, but 1G BSCCO-2223 tapes permanently degrade with twisting.

The longitudinal strain model discussed above describes very well experimental results of the critical currents of a twisted tape. In the model, the critical current of a twisted tape has been calculated with Eqs. (5.1) and (5.3) using the reported dependence of the critical current with axial strain. Twist effects on the critical current of a conventional power cable composing lapped multi tapes have been shown to be evaluated from that of a twisted single tape.

An HTS tape CICC cable could be fabricated by stacking and twisting processes of HTS flat tapes as shown in Fig. 5.5. Recently the magnetic field angle degradation (critical current anisotropy) of YBCO tapes has been improved by SuperPower using a REBCO film technique substituting either Gd and Zr for Y [5.6, 5.7]. A twisted YBCO stacked-tape cable designs can be conceived for compact high-current power conductors and high-current high-field conductors. They are illustrated in Fig. 5.6. A stacked and twisted conductor of 7 mm diameter composed of the 40 tapes may carry up to approximately 3 kA at 77 K with self field and 4.5 kA at 15 T at 4.2 K. A three-stage 9-conductor cable (3x3) of 32 mm diameter may provide 25 kA at 77 K at self field and 40 kA at 15 T at 4.2 K. In the same conductor diameter, it will be possible to make a12-conductor cable with a single stage cabling of 30 kA at 77 K at self field and 50 kA at 4.2 K at 15 T.

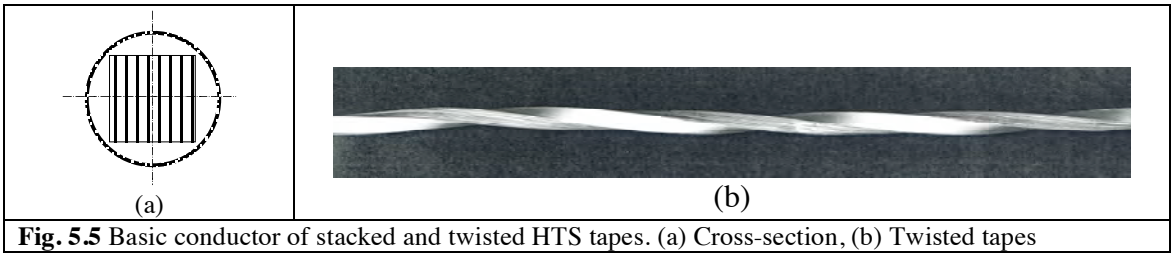

Fig. 5.5 Basic conductor of stacked and twisted HTS tapes. (a) Cross-section, (b) Twisted tapes

Fig. 5.6 Schematic illustrations.
Top: Basic conductor of 40-tape stacked and Twisted HTS tapes.
Mid: 2-stage 9-conductor HTS cable (3x3).
Bottom: 1-stage 12-conductor HTS cable.

5.6 Conclusions

Analysis of the critical current of HTS tapes under torsional twisting strains has been carried out. Torsional twist effects on a thin HTS tape has been found to be well described by the longitudinal strain model taking account of the resulting compressive strain accompanied

with the tensile longitudinal strain due to a torsional twist. The critical current of a twisted tape is obtained for the integration of the critical currents of a function of the longitudinal strain using axial strain test data of the tape. The model analysis results agree with experimental measurements on BSCCO and YBCO tapes.

The critical current of a tape of both lapped-tape and stacked-tape cables is found to be described with the critical current equation developed for a twisted single tape having the same twist pitch.

Twisted stacked tape conductors may be attractive for fusion magnet applications. More significantly conductors of this design may be advantageous for multiple other applications, as well, such as conductors of magnets for medical applications including compact synchrocyclotron and MRI (medical), SMES, and other electrical devices (transformer, fault current limiter and generators).

5.7 REFERENCES

5.1 Jin, J.X. et al, *IEEE Trans. Appl. Supercond.*, **9**, pp. 138-141 (1999).
5.2 Shin, H.S. et al., *Physica C*, **392-396**, pp. 1162-1166 (2003).
5.3 Shin, H.S. et al., *IEEE Trans. Appl. Supercond.*, **17**, pp. 3274-3277 (2007).
5.4 M. Takayasu, et al, presented at CEC-ICMC 2009, accepted for publication *Adv. Cryo. Eng*.
5.5 P.C. Michael et al., *IEEE Trans. Appl. Supercond.*, **13**, pp. 1620-1623 (2003).
5.6 Hazelton, D.W. et al., *IEEE Trans. Appl. Supercond.*, presented at ASC, Chicago, 2008.
5.7 http://superpower-inc.com: 2G field data obtained by Y. Zhang, M. Paranthaman, and A. Goyal, ORNL.

6 DEVELOPMENT OF QUENCH CODE SOLXPORT3D-QUENCH

A thermohydraulic-quench code, "Solxport3D-Quench," has been developed for superconducting magnets within power supply network circuits [6.1]. Each power supply network circuit consists of at least one superconducting magnet with parallel circuits including voltage sources, resistors or diodes as shown in Fig. 6.1. When used for analysis of a magnetic confinement fusion device, the plasma currents and passive structures eddy currents are also included in all scenarios [6.2-6.4]. The simulation starts from the superconducting state for each magnet coil. The superconducting stage switches to the quench stage if any one of the superconducting magnets becomes quenched (i.e., exceeding the current sharing temperature.) This is followed by the dumping stage after a given quench detection time. The recovery of the superconducting stage is allowed during any moment before dumping. The currents of each magnetic coil are calculated by a time-difference method. The time dependence of thermohydraulic parameters during superconducting and quench/dumping stage are also obtained by the finite element method. An arbitrary length of heating source is allowed. The size and location of each finite element are dynamically defined for each time step during quench and dumping. Fig. 6.2 shows the computer model flow diagram for the thernohydraulic quench model.

Calibrations against test data have been performed [6.5]. The code has been applied to model the quenching process in the ITER CS coils. Some examples of the computed results are shown inn Figs. 6.3-6.5.

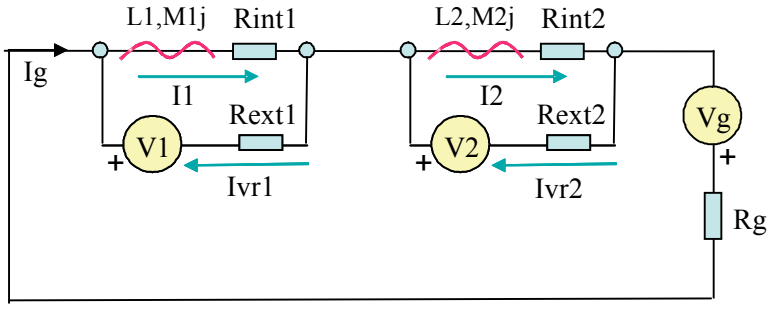

Fig. 6.1 Schematic of network circuits.

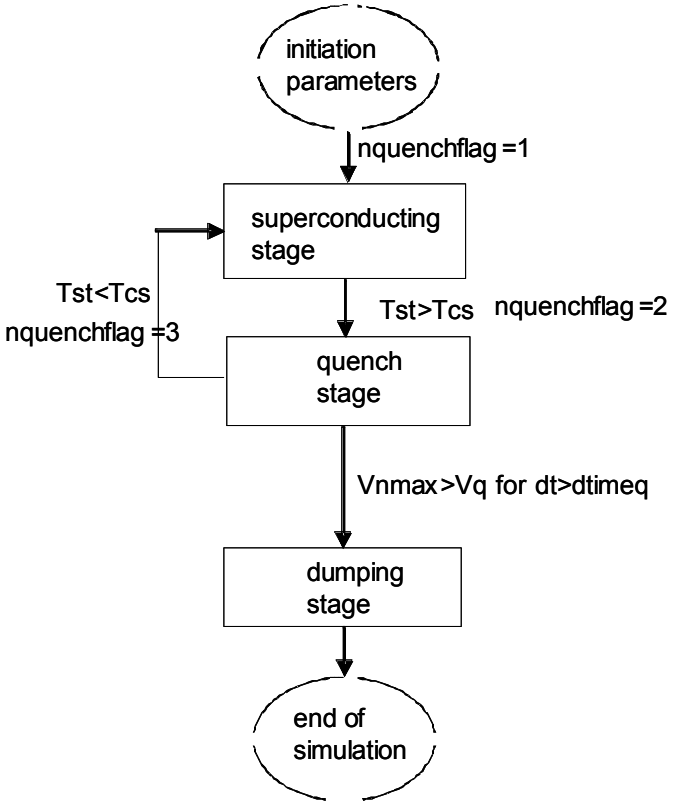

Fig. 6.2 General flow chart of the thermohydraulic-quench code.

As a next step in further development of this code we will include parameters that represent the critical properties of a 2G YBCO HTS conductor. When completed it will be used to simulate a simple HTS coil. In the future, we hope to be able to compare the code with a small experimental coil made from 2G, YBCO HTS.

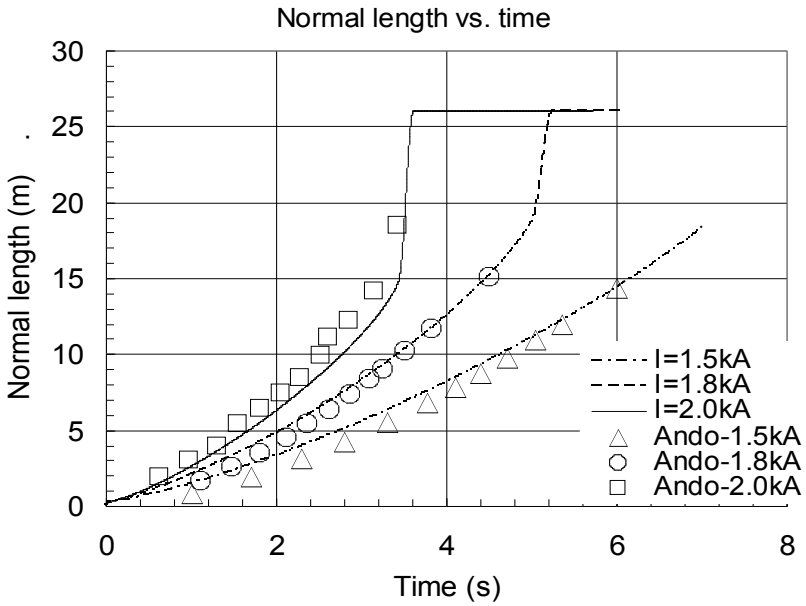

Fig. 6.3 Simulation results by SOLXPT3D-Quench for normal length compared to Ando results.

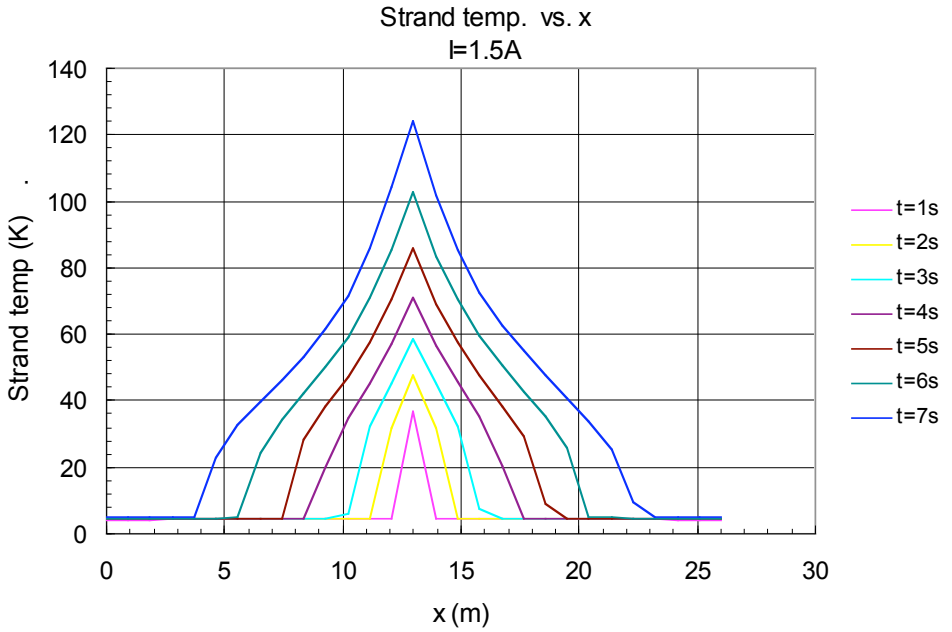

Fig. 6.4 Sample output of the simulation for T_{st} vs. cable length x.

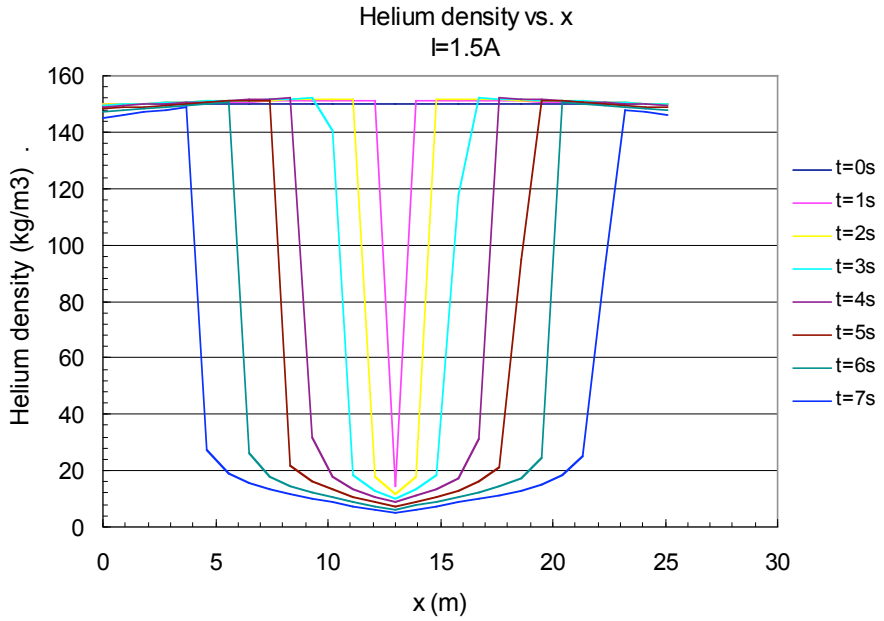

Fig. 6.5 Sample output of the simulation for He density vs. cable length x.

6.1 References

6.1 Jun Feng, Joel Schultz, and Joe Minervini, "A thermohydraulic-quenching code for superconducting magnets in network circuits," presented in CEC/ICMC09.

6.2 Jun Feng, "Circuit current solver," MAGNETBASE-MIT-FENG-112408-01, Nov. 24, 2008.

6.3 Jun Feng, "Circuit current solver after changing coil polarity," MAGNETBASE-MIT-FENG-120108-01, Dec. 1, 2008.

6.4 Jun Feng, "Simulation of the circuit networks including diodes," MAGNETBASE-MIT-FENG-120808-01, Dec. 8, 2008.

6.5 Jun Feng, "Comparison between the simulated and the analytical results," MAGNETBASE-MIT-FENG-121508-01, Dec. 15, 2008.

7 MODELING OF CABLING 3D TWISTING PATTERN

The ITER conductor is made of a superconductor cable with multi-stage twisted strands. Knowledge of the spatial structure of such a cable is essential for understanding the effect of load and strain on the performance of a superconducting cable. Unfortunately there have been no models developed so far that accurately describe such a twisted spatial structure for multistage cables. In this work we propose a twisting matrix model to accurately describe the spatial structure of a multiple-twisted superconducting cable [7.1]. The simulation results by this model agree well with the observations for pitch and orientation.

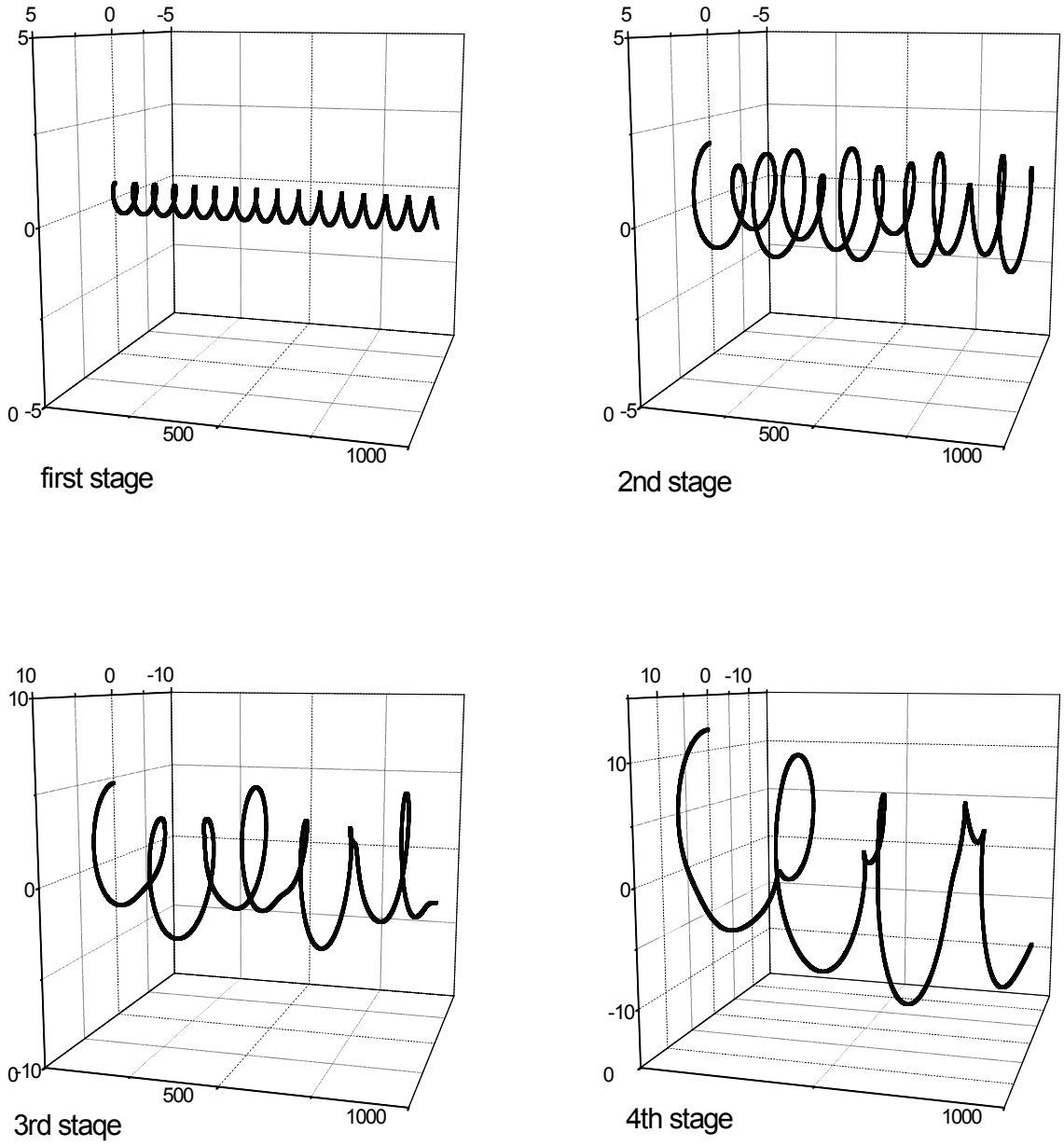

Fig. 7.1 Sample winding pattern.

7.1 References

7.1 Jun Feng, "A cable twisting model and its application in CSIC multi-stage cabling structure," accepted for publication by Fusion Engineering and Design, online available 2009.

8 STUDY OF THE JACKET MATERIALS FOR CS COILS

The jacket of a central solenoid typically experiences highly cyclic loading at 4K due to electromagnetic Lorentz forces. The jacket material must possess high strength, high ductility, and appropriate thermal expansion. There have been several candidates for such jacket. The current research includes a summary and analysis of the mechanical properties of all materials considered as candidates by the ITER IO, as well as suggestions for future work.

It is found that, for the base metal, the mechanical behavior of SS316LN as official candidate of ITER CS jacket is not well understood based on the following aspects:[8.1]

(1) Large variation of the mechanical properties is observed. It leads to large uncertainty in design (Fig. 8.2);
(2) It is well known that the CS jacket is expected to experience severe cold work during compaction and winding process. The cold work effect has significant impact on the mechanical properties. This effect has not been studied for SS316LN as a CS jacket candidate.
(3) The wall thickness of TF jacket is around 1.6mm, but that of the CS jacket is around 8mm. The effect of thickness typically appears as plain stress vs. plain strain. This effect has not been studied for the SS316LN.
(4) The large variation of properties of SS316LN is due to the combined effect of composition, cold work, aging and thickness effect. It is not understood well enough to use for the CS jacket design. Therefore, an optimization of all the factors must be performed before finalizing the official jacket design.

It is also found that, for welds, the database of the welds for in-spec JK2LB and Incoloy 908 is complete. Both alloys show a good combination of strength and ductility, but Incoloy 908 has better fatigue crack growth behavior. [8.2] – [8.3]

There is no available database for thick SS316LN welds at 4K including cold work and aging. Such thick welds simulate the butt joints of ITER CS jacket. Specifically, there are no reported data for the welds of thick SS316LN plate/conduit with CW+aging, such as optimized welding parameters, NDA results, tensile properties, fracture toughness and fatigue behavior at 4K. The only data available for SS316LN welds at 4K is for thin wall strips, which simulate ITER TF conduit, not CS. It is noted that the welding procedure of a thick plate is completely different from that for a thin sheet. NDA results about the defect distribution in thick welds may be largely different than for thin sheet welds, as well as their properties. This would have significant effect on the fatigue life of the jacket. [8.2]

Furthermore, the welds of both out-spec SS316LN reported by MIT and the SS316LN used by NHMFL all show brittle fracture features at 4K (elongation ~9%). The mechanism of this embrittlement needs further study. [8.2]

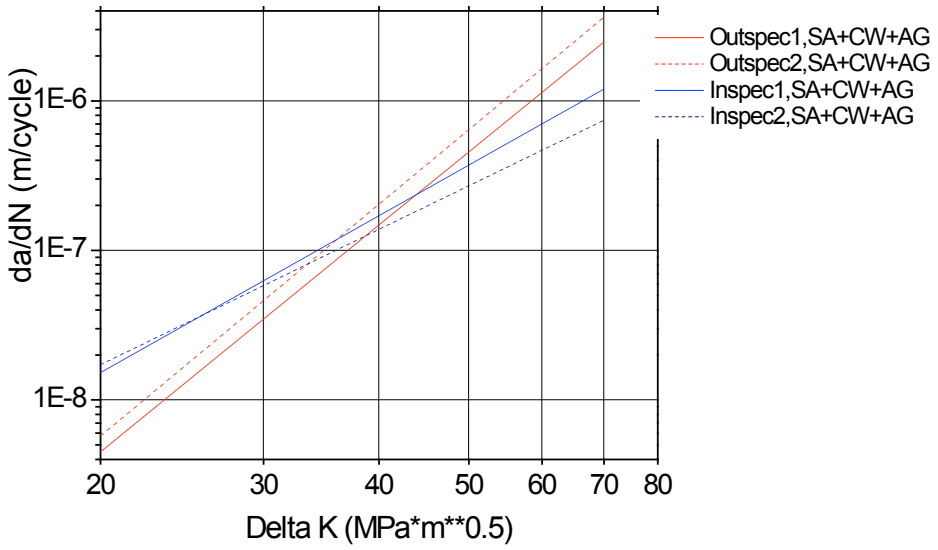

Fig. 8.1 Fatigue crack growth rate: outspec JK2LB vs. inspec JK2LB, indicating that the inspect JK2LB has higher crack growth rate if the crack size is small. [8.1]

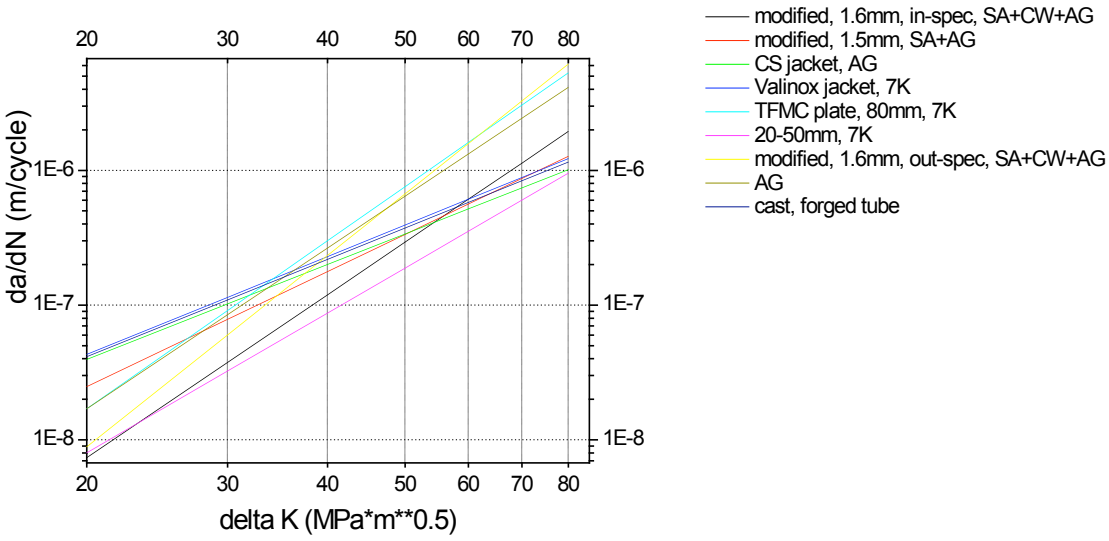

Fig. 8.2 Fatigue crack growth rate as a function of stress intensity factor range for different SS316LN, indicating a large uncertainty of the crack growth rate data.[8.1]

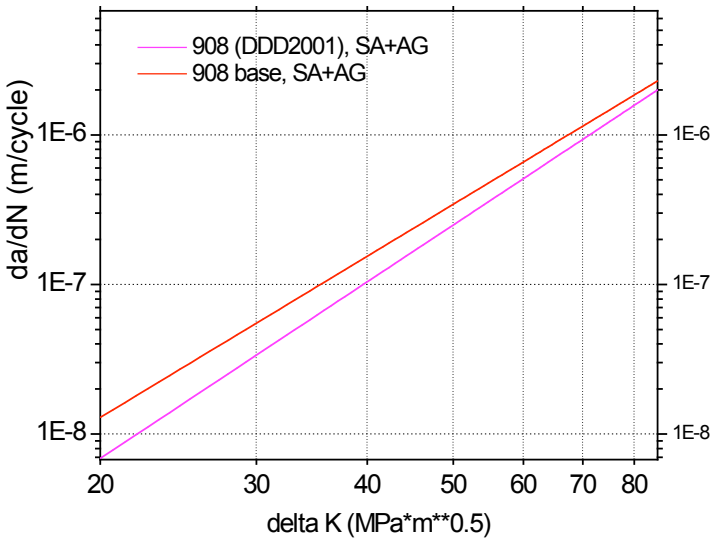

Fig. 8.3 The fatigue crack growth rate curves of Incoloy 908,[8.1] more data with SA+CW+AG are available upon request.

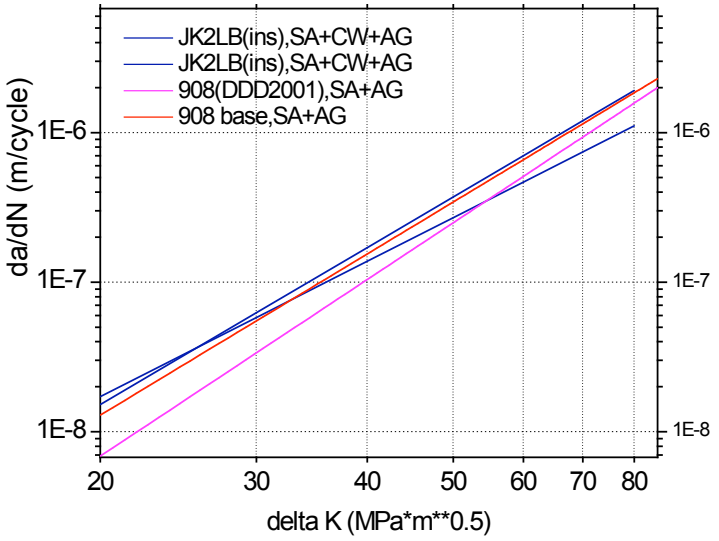

Fig. 8.4 Comparison between different CS jacket candidate materials, indicating the Incoloy 908 showing a better fatigue behavior. The data for SS316LN with CW+AG are not available. [8.1]

8.1 References

8.1 Jun Feng, "Discussion of CS Jacket Material Candidates," MAGNETBASE-MIT-FENG-072309-01, July 23, 2009.

8.2 Jun Feng, "Summary of the 4K welds properties of ITER CS conduit candidates: SS316LN, in-spec JK2LB, and Incoloy 908," MAGNETBASE-MIT-FENG-082509-01, Aug. 25, 2009.

8.3 JiHyun Kim and Jun Feng, "Weld development of Incoloy 908 in CICC superconducting magnets," to be submitted to Fusion Engineering and Design, 2009.